Energy Transfer in Nanocomposites of Zinc Oxide with Erbium and Ytterbium Oxides

I. O. Sobina[a], V. Yu. Timoshenko[a], S. V. Savilov[a], A. Yu. Steblyanko[b], and A. N. Baranov[a], *

[a] Moscow State University, Moscow, 119991 Russia
[b] Sechenov First State Medical University (Sechenov University), Russian Federation Ministry of Health, Moscow, 119991 Russia
*e-mail: anb@inorg.chem.msu.ru
Received July 1, 2021; revised July 29, 2021; accepted July 29, 2021

Abstract—Nanocomposites consisting of zinc oxide, erbium oxide, and ytterbium oxide nanoparticles have been synthesized from alcoholic solutions and thermally annealed in air. The chemical and phase compositions and microstructure of the resultant samples have been studied using X-ray diffraction, X-ray fluorescence analysis, transmission electron microscopy, X-ray microanalysis, and photoluminescence (PL) spectroscopy. The relative Yb^{3+} PL intensity in PL spectra of ZnO nanocrystals decorated with Yb_2O_3 nanocrystals has been shown to increase as twice the Yb^{3+} excitation energy is approached, which points to a cooperative ion excitation mechanism during electron excitation energy transfer from the ZnO host. If both Er^{3+} and Yb^{3+} ions are present in the rare-earth (RE) oxide phase, the Yb^{3+} PL intensity is lower, attesting to a competition between Er^{3+} and Yb^{3+} excitation processes during energy transfer from ZnO to the RE ions. The results obtained in this study pave the way to the use of ZnO- and RE-based nanocomposites for making luminescent sources emitting in a wide spectral range.

Keywords: nanocrystals, nanocomposites, zinc oxide, erbium, ytterbium, photoluminescence
DOI: 10.1134/S002016852112013X

INTRODUCTION

Rare-earth (RE) ions have a small optical absorption coefficient, so various sensitizers with broadband absorption, for example, organic ligands [1] or semiconductor hosts [2], should be used to effectively excite them.

One well-known sensitizer of RE ions is a ZnO host, which was successfully used for energy transfer to RE ions after absorption of external UV radiation [3, 4]. Owing to its wide band gap (on the order of 3.3 eV), zinc oxide exhibits efficient luminescence in the UV spectral region, due to excitonic states, and in the visible range, due to defect states [5, 6].

The ability to extend the luminescence spectrum of zinc oxide to the near-IR spectral region is of importance for many applications, for example, for photon energy down-conversion in solar cells [7] and biovisualization in the peak transmission region of biological tissue with the use of IR-luminescent markers [8]. Yb^{3+} ions are known to typically require resonance excitation conditions because they have only two levels for excitation. The presence of Yb_2O_3 nanoparticles on the surface of ZnO nanoparticles can improve Yb^{3+} excitation efficiency for subsequent emission in the near-IR spectral region [8]. The efficient Yb^{3+} excitation in such nanocomposites can be accounted for in terms of energy transfer from photoexcited ZnO nanoparticles by the Förster mechanism, in particular by the "photon cutting" mechanism, where excitation is simultaneously transferred in the form of a high-energy photon from the ZnO host to two Yb^{3+} ions, resulting in emission of two low-energy photons [8—11].

The ability to increase intensity in the visible spectral region via photon energy upconversion can be used in optoelectronics, biovisualization, and IR detectors [12, 13]. This can be done by using a pair of ions: Er^{3+} + Yb^{3+} [14—17]. Owing to the existence of coinciding excitation channels for levels of Er^{3+} and Yb^{3+} ions at a wavelength near 980 nm (the $^4I_{11/2} \to {}^4I_{15/2}$ transition with a wavelength of 988 nm and $^4F_{7/2} \to {}^4I_{11/2}$ transition with a wavelength of 964 nm in Er^{3+} and the $^4F_{5/2} \to {}^4F_{7/2}$ transition with a wavelength near 980 nm in Yb^{3+}), they can exchange energy [18]. In particular, energy transfer from Yb^{3+} to Er^{3+} ions is possible, followed by upconversion excitation of Er^{3+} levels.

In this study, $ZnO/(Er,Yb)_2O_3$ nanocomposites were prepared via synthesis from alcoholic solutions, a

Table 1. Elemental composition of the samples according to XRF data

Sample	ZOEr1Yb1	ZOEr1Yb5	ZOEr2Yb2	ZOEr2Yb5
at % Zn	96.6 ± 0.1	90.5 ± 0.1	94.9 ± 0.1	90.8 ± 0.1
at % Er	2.0 ± 0.1	1.8 ± 0.1	3.6 ± 0.1	2.9 ± 0.1
at % Yb	1.4 ± 0.1	7.7 ± 0.1	1.5 ± 0.1	6.3 ± 0.1

technique used previously to demonstrate efficient energy transfer from ZnO to individual Yb^{3+} ions [8]. We aimed to study photoluminescence (PL), mechanisms of energy transfer from the ZnO semiconductor host to Er^{3+} and Yb^{3+} ions, and mechanisms of energy exchange between the RE ions in such nanocomposites.

The objectives of this work were to assess the effect of the composition of zinc oxide-based nanocomposites on ytterbium and erbium luminescence efficiency and study the excitation of the RE ions at different photon energies, which was expected to allow us to understand the potential of such nanocomposites for use in the fabrication light-emitting devices in a wide spectral range.

EXPERIMENTAL

In our preparations, we used the following starting materials: $Zn(CH_3COO)_2 \cdot 2H_2O$ (Aldrich), $Er(NO_3)_3 \cdot 5H_2O$ (reagent grade), $Yb(NO_3)_3 \cdot 4H_2O$ (reagent grade), $LiOH \cdot H_2O$ (reagent grade), and CH3OH (for chromatography).

$ZnO/(Er,Yb)_2O_3$ nanocomposites were prepared using alcoholic solutions and then annealed in air at 700°C as described previously [8]. Synthesis was carried out from alcoholic solutions in methanol according to the following reaction scheme:

$$\{Zn(CH_3COO)_2 + xEr(NO_3)_3 + yYb(NO_3)_3\}$$
$$+ (2 + 3(x + y))LiOH \rightarrow ZnO/(xEr + yYb)O_{1.5}$$
$$+ 2CH_3COOLi + 3H_2O + 3(x + y)LiNO_3,$$

where x is the atomic fraction of Er and y is the atomic fraction of Yb. This method allowed us to obtain $ZnO/(Er,Yb)_2O_3$ nanoparticles, which were stable in the alcoholic solution owing to the acetate groups adsorbed on their surface.

The designation of our samples, for example ZOEr2Yb2, specifies the mole percentages of the RE metals in zinc oxide (2 mol % Er and 2 mol % Yb).

The elemental composition of the as-prepared samples was determined by X-ray fluorescence (XRF) analysis with a DR-2 Radian instrument at a voltage of 15 kV and current of 3 mA. We analyzed relative signal intensities and the corresponding atomic fractions of elemental Zn, Er, and Yb.

The $ZnO/(Er,Yb)_2O_3$ samples were characterized by transmission electron microscopy (TEM) on a JEOL JEM-2100F (Japan) operated at an accelerating voltage of 200 kV and equipped with a spherical and chromatic aberration corrector, placed in transmission mode, and an energy dispersive X-ray analyzer for determining elemental compositions. The TEM specimen preparation procedure included ultrasonication of a weighed amount (1 mg) of a sample in water for 15 min. After that, a droplet of the resultant suspension was applied to a copper grid precoated with polyvinyl formal.

X-ray diffraction patterns were collected on a Rigaku D/MAX 2500 diffractometer (CuK_α radiation).

PL spectra of the samples were measured at room temperature in air on a Mightex spectrometer under excitation by various cw laser sources at wavelengths of 365, 405, 465, 532, and 650 nm with output powers of 300, 500, 100, 50, and 180 mW, respectively. Powder samples were applied to metallic platelets and secured with an alcoholic solution (ethanol).

RESULTS AND DISCUSSION

The elemental compositions of the samples determined by XRF analysis on the whole correlate with the intended ones (Table 1).

According to X-ray diffraction data (Fig. 1), the synthesized nanoparticles consisted largely of a well-crystallized ZnO phase (wurtzite structure, sp. gr. $P6_3mc$, card no. 36-1451) and a solid solution between erbium and ytterbium oxides.

Table 2 lists the calculated lattice parameters and crystallite size of ZnO and the RE oxides. There is no clear correlation between the lattice parameters of ZnO and the percentages of the REs, which provides indirect evidence that there are no RE cations in the zinc oxide lattice [8, 9]. Varying the relative Er_2O_3 and Yb_2O_3 concentrations leads to a linear shift of the reflections from the solid solution between the RE oxides, in which according to the calculated lattice parameters the end-members are Er_2O_3 (cubic structure, sp. gr. $Ia3$, card no. 8-50) and Yb_2O_3 (cubic structure, sp. gr. $Ia3$, card no. 41-1106).

The crystallite size of the samples, as determined from the width of diffraction peaks, ranged from 40 to
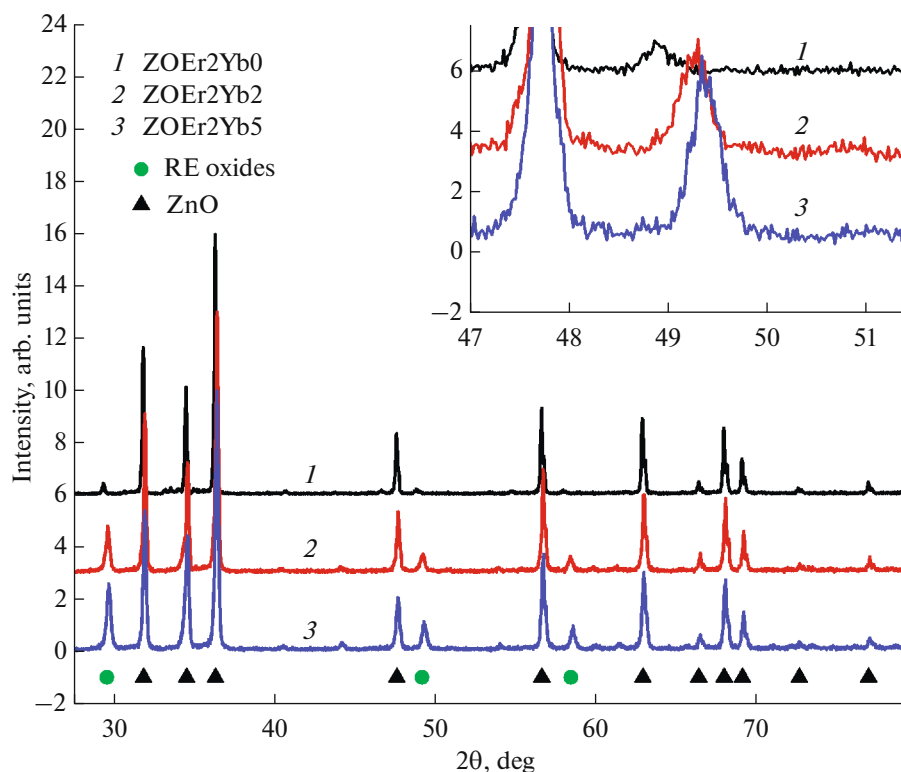
Fig. 1. X-ray diffraction patterns of the ZOEr2Yb samples containing 0−5 at % Yb.

70 nm for ZnO and from 14 to 48 nm for the RE oxides. The nanocrystal size in pure Er_2O_3 was 43−48 nm and that in the solid solutions was found to decrease with increasing Yb_2O_3 content. There was no clear correlation between the nanocrystal size of ZnO and the total RE oxide concentration.

In the ZOEr2Yb5 sample, the average crystallite size of ZnO determined from the corresponding diffraction peaks by the Williamson−Hall method was 40.7 ± 5.1 nm ($\varepsilon = 5.6 \times 10^{-4}\%$), approaching that determined using the Scherrer formula. Therefore, the lattice strain in the nanocrystals was low, and the width of the diffraction peaks was determined mainly by particle-size broadening.

According to TEM data, the ZOEr2Yb5 nanoparticles annealed at 700°C were nearly spherical in shape and ranged in size from 80 to 500 nm in the case of particles darker in contrast and from 10 to 80 nm in the case of lighter particles (Fig. 2). It is reasonable to assume that the darker contrast corresponds to ZnO particles, and the lighter one, to the RE oxides, which is consistent with the crystallite sizes evaluated from the X-ray diffraction data if we assume that the large ZnO particles can consist of several crystallites. This assumption is supported by the characteristic X-ray

Table 2. Crystallite size in the samples as determined from X-ray diffraction data using the Scherrer formula

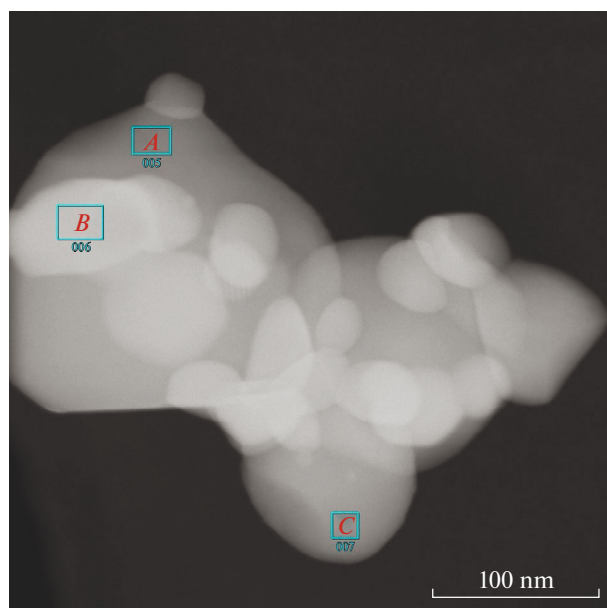| Sample	a, nm	c, nm	D, nm	a, nm	D, nm
	ZnO			$(Er,Yb)_2O_3$	
ZOEr1Yb1	3.2526(2)	5.2110(4)	48 ± 9	10.488(3)	31 ± 15
ZOEr1Yb5	3.2504(6)	5.212(2)	40 ± 6	10.4332(3)	14 ± 6
ZOEr2Yb2	3.2528(1)	5.2099(2)	54 ± 9	10.501(2)	34 ± 13
ZOEr2Yb5	3.2526(2)	5.2100(6)	42 ± 7	10.461(3)	30 ± 14
ZOEr1	3.2516(1)	5.2073(2)	66 ± 17	10.538(2)	43 ± 29
ZOEr2	3.2534(8)	5.212(3)	71 ± 8	10.543(1)	48 ± 36

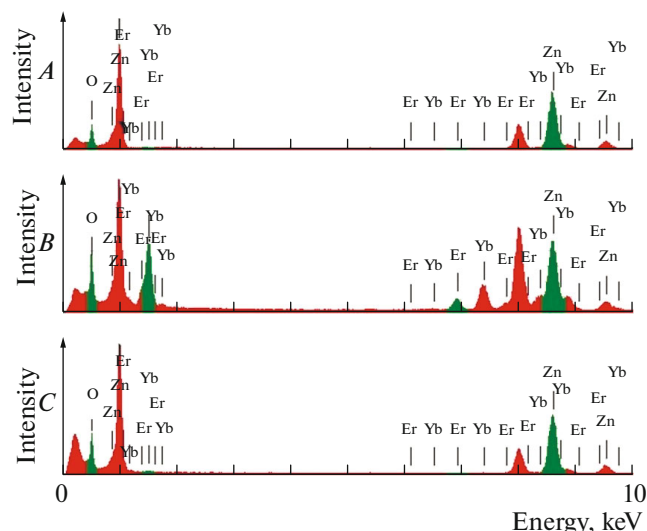**Fig. 2.** TEM image of the ZOEr2Yb5 sample.

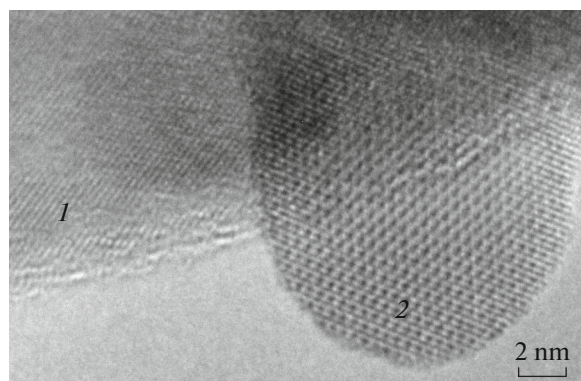**Fig. 3.** Characteristic X-ray spectra of the outlined regions in the TEM image in Fig. 2.

Fig. 4. High-resolution TEM image of the ZOEr2Yb5 sample: (*1*) ZnO, (*2*) RE oxides.

Fig. 5. PL spectra of the ZnO-based nanocomposites differing in Yb content (excitation wavelength of 465 nm).

spectra in Fig. 3. It is well seen that the large (dark) nanoparticles correspond to ZnO (regions *A* and *C*), whereas the small (light) nanoparticles correspond to a solid solution between the RE oxides (region *B*). Note that other images of characteristic X-ray spectra also always contained peaks of both Er and Yb, confirming that Er_2O_3 and Yb_2O_3 were present in a single crystal lattice. The same is evidenced by the TEM image in Fig. 4. It is worth noting that the nanoparticles seen in the image differ in crystal lattice: the larger nanoparticle has a hexagonal structure (ZnO) and the smaller one has a cubic structure (RE oxides).
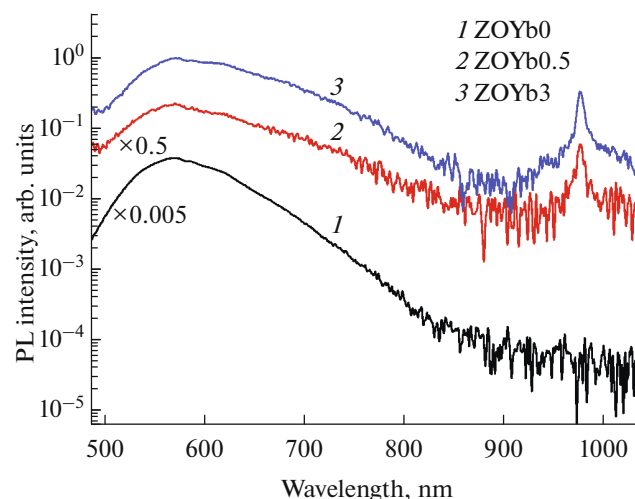
According to the data in Fig. 5, the PL spectra of the ZnO-based nanocomposites contain a broad band peaking near 650−700 nm, which is due to electronic transitions in defect states, and a narrow line near 980 nm, corresponding to the Yb^{3+} $^2F_{5/2} \rightarrow ^2F_{7/2}$ transition. As the Yb^{3+} PL line emerges, the intensity of the PL band due to defect states decreases. This finding can be interpreted as due to excitation of Yb^{3+} ions via energy transfer from photoexcited ZnO nanoparticles.

The normalized Yb^{3+} PL intensity in the ZOYb0.5 sample is a nonmonotonic function of excitation photon energy, with a well-defined maximum (Fig. 6).
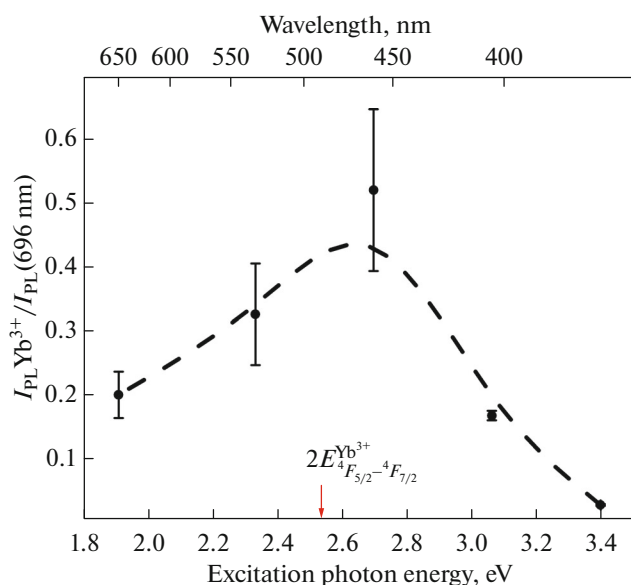
Fig. 6. Ratio of the Yb^{3+} PL intensity to the intensity of the defect-related band at 696 nm as a function of excitation wavelength (cw laser) for the ZOYb0.5 nanocomposite.

Fig. 7. PL spectra of the ZOEr1 nanocomposites differing in Yb content (excitation wavelength of 405 nm).

This indicates that Yb^{3+} excitation efficiency increases considerably as the excitation photon energy approaches twice the energy of the Yb^{3+} levels: 2.52 eV. This effect suggests that the most efficient excitation of Yb^{3+} ions occurs by the "photon cutting" mechanism, where excitation energy is transferred from the photoexcited ZnO host to two Yb^{3+} ions.

Figure 7 demonstrates that, on the addition of Yb^{3+} ions to the ZOEr1 nanocomposite, the peak at a wavelength near 980 nm becomes sharper and shifts to shorter wavelengths. This suggests that this PL peak is the sum of contributions from Er^{3+} and Yb^{3+} ions and that their PL is dominated by the ions whose concentration is higher.

As the Er concentration increases to 2 at %, the 980-nm peak exhibits qualitatively similar behavior, independent of Yb concentration (Fig. 8). It is worth noting that, as the Yb concentration increases from 2 to 5 at %, weak features emerge in the PL spectrum in the range 640–690 nm, which are attributable to the Er^{3+} $^4F_{9/2} \rightarrow {}^4I_{15/2}$ transition (the $^4F_{9/2}$ level is split). This points to a cooperative energy transfer mechanism, for example, from a few (two) Yb^{3+} ions to Er^{3+}.

In Fig. 9, only peaks of Er^{3+} ions are seen at equal Er and Yb concentrations. As the Yb concentration increases, the peaks of Er^{3+} ions disappear and a peak of Yb^{3+} ions emerges, which is considerably weaker than in the absence of the Er_2O_3 phase (Fig. 9, black line). This indicates that there is a competition
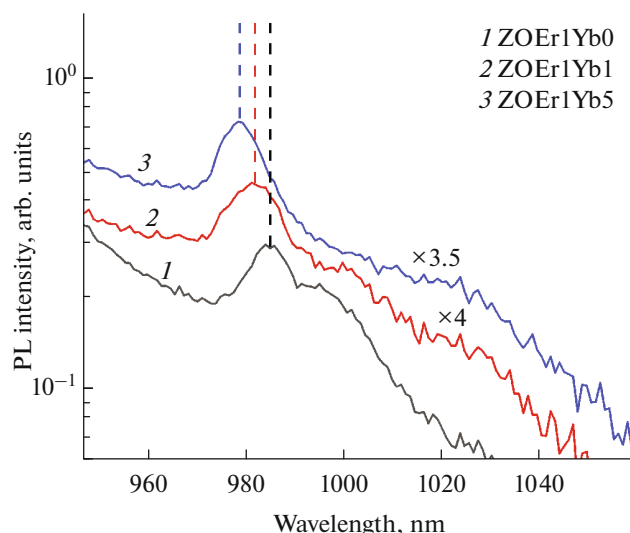
between Er^{3+} and Yb^{3+} excitation processes during energy transfer from the photoexcited ZnO host.

Thus, we are led to propose the following mechanism of PL in the $ZnO/(Er,Yb)_2O_3$ nanocomposites (Fig. 10): Owing to the presence of defect-related levels, the photoexcited ZnO host passes on energy to Er^{3+} and Yb^{3+} ions via the Förster dipole–dipole mechanism. Note that the latter process can involve an energy loss or follow the "photon cutting" mechanism. The RE ions can also exchange energy with each other by the Förster mechanism through transitions similar in energy at wavelengths near 980 nm ($^4I_{11/2} \rightarrow$
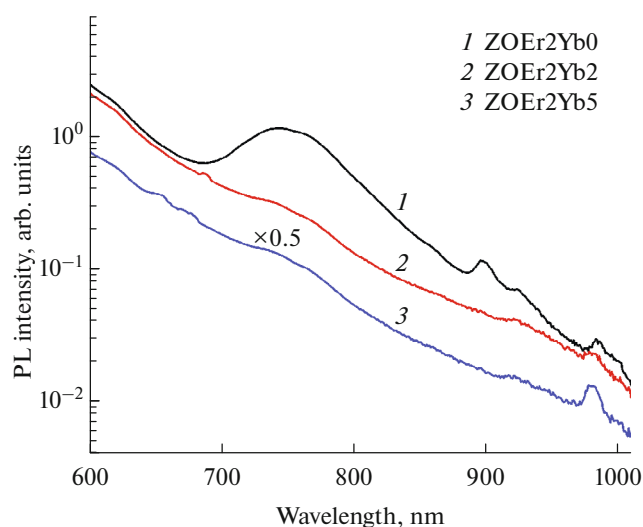

Fig. 8. PL spectra of the ZOEr2 nanocomposites differing in Yb content (excitation wavelength of 405 nm).
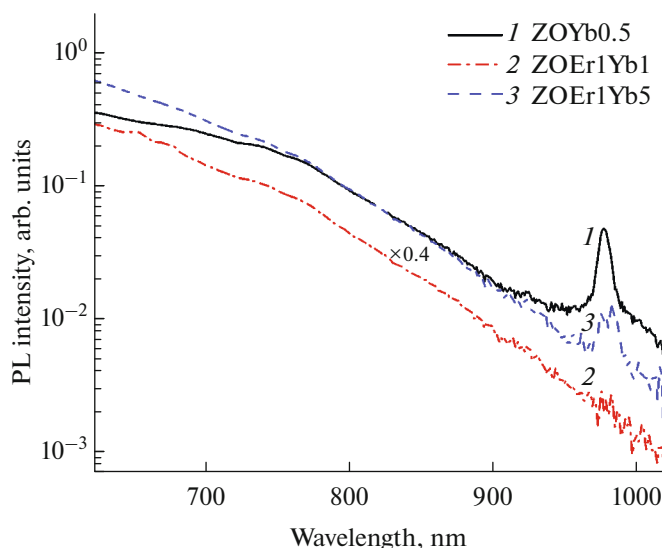
Fig. 9. PL spectra of the ZnO-based nanocomposites differing in Er and Yb contents (excitation wavelength of 465 nm).
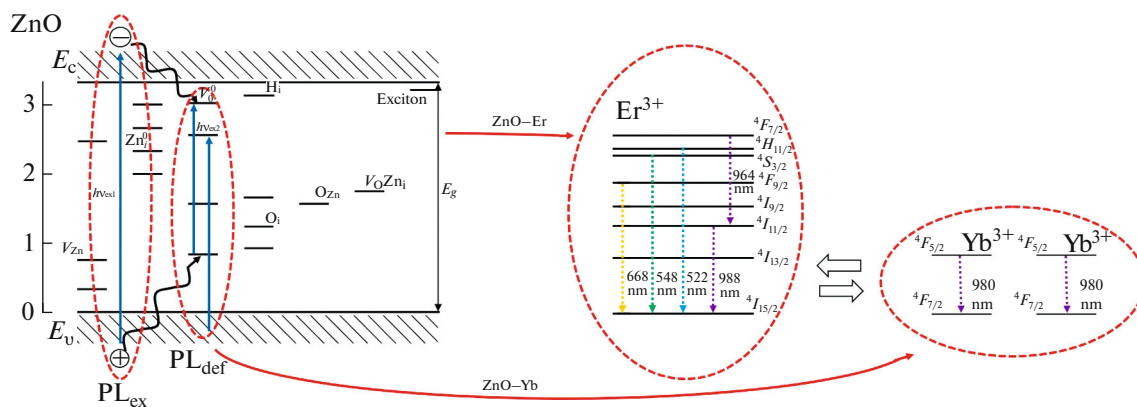

Fig. 10. Schematic of excitation and PL in the ZnO/(Er,Yb)$_2$O$_3$ nanocomposites.

$^4I_{15/2}$ and $^4F_{7/2} \rightarrow {}^4I_{11/2}$ transitions in the Er^{3+} ions and $^4F_{5/2} \rightarrow {}^4F_{7/2}$ transition in the Yb^{3+} ions). Energy transfer from Er^{3+} ions is hindered first because the energy separation between the Er^{3+} levels is slightly smaller than that in the case of Yb^{3+} and second because Er^{3+} has lower energy levels, to which electrons relax ($^4I_{13/2}$ and others). At some wavelengths and some relationships between the RE concentrations, we observe an upconversion energy transfer from Yb^{3+} to Er^{3+} ions, followed by electron relaxation through energy levels and emission, in particular, that in the range 640–690 nm. On the whole, interaction between the RE cations is weak, and there is mainly a competition between processes of RE ion excitation from the ZnO host.

CONCLUSIONS

We have studied structural properties and PL of ZnO nanoparticles with erbium oxide and ytterbium oxide nanoparticles deposited on them. The most efficient Yb^{3+} PL at a wavelength near 980 nm has been observed in the ZnO nanocrystals decorated with Yb$_2$O$_3$ nanocrystals, at an excitation photon energy near twice the Yb^{3+} excitation energy. This points to simultaneous energy transfer from photoexcited ZnO nanocrystals to two Yb^{3+} ions. The addition of Er reduces the Yb^{3+} PL intensity and causes emission lines of Er^{3+} ions to emerge.

The results obtained in this study are of interest for understanding processes underlying energy transfer

from a semiconductor host to RE ions and for making light sources emitting in a wide spectral range.

FUNDING

CONFLICT OF INTEREST

The authors declare that they have no conflicts of interest.

REFERENCES

1. Katkova, M.A., Vitukhnovskii, A.G., and Bochkarev, M.N., Coordination compounds of rare-earth metals with organic ligands for electroluminescent diodes, *Russ. Chem. Rev.,* 2005, vol. 74, no. 12, pp. 1089−1109.
https://doi.org/10.1070/RC2005v074n12ABEH002481

2. Chen, D., Wang, Y., and Hong, M., Lanthanide nanomaterials with photon management characteristics for photovoltaic application, *Nano Energy,* 2012, vol. 1, no. 1, pp. 73−90.
https://doi.org/10.1016/j.nanoen.2011.10.004

3. Du, Y.P., Zhang, Y.W., Sun, L.D., and Yan, C.H., Efficient energy transfer in monodisperse Eu-doped ZnO nanocrystals synthesized from metal acetylacetonates in high-boiling solvents, *J. Phys. Chem. C,* 2008, vol. 112, no. 32, pp. 12234−12241.
https://doi.org/10.1021/jp802958x

4. Bang, J., Yang, H., and Holloway, P.H., Enhanced luminescence of $SiO_2:Eu^{3+}$ by energy transfer from ZnO nanoparticles, *J. Chem. Phys.,* 2005, vol. 123, no. 8, paper 084709.
https://doi.org/10.1063/1.2007647

5. Kumar, E.S., Singh, S., and Rao, M.S.R., Zinc oxide: the versatile material with an assortment of physical properties, *Springer Ser. Mater. Sci.,* 2014, vol. 180, pp. 1−38.
https://doi.org/10.1007/978-81-322-1160-0_1

6. Karipidis, T.K., Chukichev, M.V., Maltsev, V.V., Volkova, E.A., and Leonyuk, N.I., Effect of annealing on cathodoluminescence of synthetic zincite single crystals, *Inorg. Mater.,* 2009, vol. 46, no. 1, pp. 43−46.
https://doi.org/10.1134/S0020168509010075

7. Balestrieri, M., Ferblantier, G., Colis, S., Schmerber, G., Ulhaq-Bouillet, C., Muller, D., Slaoui, A., and Dinia, A., Structural and optical properties of Yb-doped ZnO films deposited by magnetron reactive sputtering for photon conversion, *Sol. Energy Mater. Sol. Cells,* 2013, vol. 117, pp. 363−371.
https://doi.org/10.1016/j.solmat.2013.06.032

8. Shalygina, O.A., Nazarov, I.V., Baranov, A.V., and Timoshenko, V.Yu., Structure and photoluminescence properties of zinc oxide/ytterbium oxide nanocomposites, *J. Sol−Gel Sci. Technol.,* 2017, vol. 81, no. 2, pp. 333−337.
https://doi.org/10.1007/s10971-016-4258-y

9. Shestakov, M.V., Baranov, A.N., Tikhomirov, V.K., Zubavichus, Ya.V., Kuznetsov, A.S., Veligzhanin, A.A., Kharin, A.Yu., Rösslhuber, R., Timoshenko, V.Yu., and Moshchalkov, V.V., Energy-transfer luminescence of a zinc oxide/ytterbium oxide nanocomposite, *RSC Adv.,* 2012, vol. 2, no. 23, pp. 8783−8788.
https://doi.org/10.1039/C2RA20755A

10. Dexter, D.L., Possibility of luminescent quantum yields greater than unity, *Phys. Rev.,* 1957, vol. 108, no. 3, pp. 630−633.
https://doi.org/10.1103/PhysRev.108.630

11. Shestakov, M.V., Tikhomirov, V.K., Kirilenko, D.A., Kuznetsov, A.S., Chibotaru, L.F., Baranov, A.N., Tendeloo, G., and Moshchalkov, V.V., Quantum cutting in Li (770 nm) and Yb (1000 nm) co-dopant emission bands by energy transfer from the ZnO nano-crystalline host, *Opt. Express,* 2011, vol. 19, no. 17, pp. 15955−15964.
https://doi.org/10.1364/OE.19.015955

12. Kolesov, R., Xia, K., Reuter, R., Stöhr, R., Zappe, A., Meijer, J., Hemmer, P.R., and Wrachtrup, J., Optical detection of a single rare-earth ion in a crystal, *Nat. Commun.,* 2012, vol. 3, no. 1, paper 1029.
https://doi.org/10.1038/ncomms2034

13. Gamelin, D.R. and Gudel, H.U., Upconversion processes in transition metal and rare earth metal systems, *Bern. Top. Curr. Chem.,* 2001, vol. 214, pp. 1−56.
https://doi.org/10.1007/3-540-44474-2_1

14. Auzel, F., Upconversion and anti-Stokes processes with *f* and *d* ions in solids, *Chem. Rev.,* 2004, vol. 104, no. 1, pp. 139−173.
https://doi.org/10.1021/cr020357g

15. Sokolov, S.A., Rösslhuber, R., Zhigunov, D.M., Latukhina, N.V., and Timoshenko, V.Yu., Photoluminescence of rare earth ions (Er^{3+}, Yb^{3+}) in a porous silicon matrix, *Thin Solid Films,* 2014, vol. 562, pp. 462−466.
https://doi.org/10.1016/j.tsf.2014.03.084

16. Huang, X., Han, S., Huang, W., and Liu, X., Enhancing solar cell efficiency: the search for luminescent materials as spectral converters, *Chem. Soc. Rev.,* 2013, vol. 42, no. 1, pp. 173−201.
https://doi.org/10.1039/C2CS35288E

17. He, S., Xia, H., Zhang, J., Zhu, Y., and Chen, B., Highly efficient up-conversion luminescence in Er^{3+}/Yb^{3+} co-doped $Na_5Lu_9F_{32}$ single crystals by vertical Bridgman method, *Sci. Rep.,* 2017, vol. 7, no. 1, paper 8751.
https://doi.org/10.1038/s41598-017-09222-0

18. Volkova, E.A., Ksenofontov, D.A., Maltsev, V.V., Leonyuk, N.I., Kabalov, Yu.K., Barilo, S.N., Bychkov, G.L., Tolstik, N.A., and Kuleshov, N.V., Liquid-phase epitaxy of single-crystal erbium−ytterbium codoped $YAL_3(BO_3)_4$ layers as key components of planar waveguides, *Inorg. Mater.,* 2011, vol. 47, no. 9, pp. 979−982.
https://doi.org/10.1134/S002016851109024X

Translated by O. Tsarev